coatings

MDPI

Article

Surface Functionalization of Activated Carbon with Phosphonium Ionic Liquid for CO_2 Adsorption

Xiaodong He, Jiamei Zhu *, Hongmin Wang, Min Zhou and Shuangquan Zhang

School of Chemical Engineering and Technology, China University of Mining and Technology, Xuzhou 221116, China; 18361227595@163.com (X.H.); m15505198380@163.com (H.W.); zmmcumt@126.com (M.Z.); cumtzsqq@126.com (S.Z.)

* Correspondence: zhujiamei1991@cumt.edu.cn; Tel.: +86-516-8359-1109

Received: 28 August 2019; Accepted: 16 September 2019; Published: 18 September 2019

Abstract: Immobilization of phosphonium ionic liquid (IL) onto activated carbon (AC) was synthesized via grafting and impregnated methods, and the modified materials were analyzed via Fourier-transform infrared spectroscopy (FTIR), X-ray diffraction, thermal gravity analysis, scanning electron microscope, pore structure and CO_2/N_2 adsorption selectivity. The effect of the gas flow rate (100–500 mL/min) and adsorption pressure (0.2–0.6 MPa) on the dynamic adsorption behavior of mixture gas containing 15 vol.% CO_2 and 85 vol.% N_2 was explained using a breakthrough method. By analyzing the breakthrough curves, the adsorption capacity was determined. The results show that surface functionalization of activated carbon with phosphonium ionic liquid is conducive to improving CO_2/N_2 selectivity, especially ionic liquid-impregnated film. The different adsorption behaviors of impregnated and grafted adsorbents are observed under various conditions. The grafted AC had better CO_2 adsorption and mass transfer due to a lower blockage of pores by ionic liquid.

Keywords: activated carbon; ionic liquid coating; adsorption; surface modification

1. Introduction

CO_2 capture is one of the most cost-effective and practical methods to mitigate global warming effects. Conventional CO_2 capture technologies mainly include absorption, adsorption and membrane separation [1–3]. The use of traditional adsorbents such as activated carbon (AC), silica and zeolites for CO_2 separation has grown steadily, primarily because adsorption is energy efficient with fast adsorption/desorption rates and a reduction of corrosion [4]. As a porous carbonaceous adsorbent, AC has a better sorption ability than other adsorbents, and thus its energy consumption during regeneration is relatively low, which is why it is the main adsorbent used in industrial adsorption [5]. Nowadays, enormous research effort is devoted to modifying the surface and pore structures of activated carbon in order to enhance its adsorption capacity for CO_2 [6–8]. However, AC as an adsorbent presently exhibits low CO_2 adsorption selectivity, especially in the presence of water vapor in the flue gas [9]. These hinder its practical applications in industry CO_2 capture processes.

Ionic liquid (IL) has many desirable features for CO_2 capture processes including high selectivity, extreme non-volatility, thermally stability and tunable properties [10,11]. It can be classified into four cation categories, including imidazolium, pyridinium, ammonium and phosphonium [12]. Among them, phosphonium-based IL has better advantages in some aspects. For example, it has good thermal stability [13], and its density is generally lower than that of water [14,15], which facilitates its separation from water layers containing inorganic by-products during the production process. Nevertheless, the high viscosity of IL leads to a slow mass transfer rate, which seriously affects the adsorption performance of CO_2 [16,17]. Furthermore, the high cost of IL is a major obstacle to its use in industrial processes.

Coating IL onto high-surface porous materials may not only overcome the problem of selectivity of the supporter, but exploit the advantages of a low cost and fast diffusivity. Moreover, immobilized IL can not only increase the interface between IL and CO_2, but can also form a thin layer of IL phase to overcome the problem of a low mass transfer rate (due to the high viscosity of IL). The IL-functionalized carrier materials are prepared by the grafting and impregnation methods. The grafting method can provide many favorable conditions for its application in adsorption, catalysis and organic synthesis [18], while the impregnation method is easy to operate and suitable for most ILs. The two methods have their own advantages and disadvantages regarding cost, operation, IL loading and pore plugging, so that the different effects on the separation performance of CO_2 are worthy of research.

IL-modified porous materials created by physical adsorption and chemical bonding for CO_2 adsorption have attracted great interest in applications for pre- and post-combustion capture during recent years [19,20]. Kinik [21] studied the selectivity to CO_2/CH_4 and CO_2/N_2 on 1-n-butyl-3-methylimidazolium hexafluorophosphate, [Bmim][PF_6], which is double by incorporation into zeolitic imidazolate framework-8 (ZIF-8) by the impregnated method. Ruckart [22] reported the use of six ILs containing the taurinate anion and paired with five tetraalkylammonium cations (where alkyl = methyl, ethyl, propyl, butyl and hexyl) and a tetrabutyl phosphonium cation, which were used to impregnate ordered mesoporous silica (SBA-15). The results showed that the adsorption capacity of IL-modified SBA is 1.2 to 1.5 times that of bare SBA (0.7 mmol·g^{-1}) at 25 °C and 0.105 MPa. Alessandro Erto [23] presented the finding that the CO_2 adsorption capacity of [Hmim][BF_4]/AC (2.01 mol·kg^{-1}) is less than bare AC (2.51 mol·kg^{-1}) at 80 °C and 0.03 MP, while that of [Emim][Gly]/AC is better (3.19 mol·kg^{-1}). Many studies have proven that appropriate IL-functionalization on AC is beneficial to the increase of CO_2 adsorption performance.

To further improve CO_2 adsorption properties of adsorbents, the present work functionalized novel hydrophobic phosphonium IL on the surface of AC using the impregnation and grafting methods. The effects of IL loading and the pore structure of IL-modified AC on CO_2/N_2 selectivity were investigated in detail. Dynamic adsorption properties at varied conditions of simulated flue gas containing 15 vol.% CO_2 and 85 vol.% N_2 for this novel IL-modified sorbent were measured to evaluate their potential for industry applications.

2. Materials and Methods

2.1. Materials

Coconut-shell activated carbon (particle size: 10–28 mesh) was purchased from Hainan Xing Guang Activated Carbon Factory (Hainan, China); 3-chloropropyltriethoxysilane (purity: 97%) was purchased from Beijing Fengtuo Chem Co, Ltd. (Beijing, China); Tri-n-octylphosphine (purity: 97%) was purchased from Stream Chemicals, Inc. (Cambridge, UK); and bistrifluoromethanesulfonimide lithium (purity: 99%) was purchased from J&K Scientific (Beijing, China). Others were analytical reagents and were used directly.

2.2. Synthesis

2.2.1. IL-Modified AC by Impregnated Method

AC was pretreated with 5 mol/L nitric acid at 25 °C for 4 h. It was then washed with distilled water until neural and dried at 90 °C under vacuum for 8 h before further use. The pretreated AC is referred as bare AC in the following text.

A similar process [24] was used to prepare the phosphonium chlorine salt via the nucleophilic displacement of 3-chloropropyltriethoxysilane with tri-n-octylphosphine in anhydrous toluene at 110 °C for 40 h. Then, phosphonium bistrifluoromethanesulfonimide (as shown in Figure 1) was synthesized via an anion exchange reaction. Phosphonium chloride was stirred with an aqueous solution of bistrifluoromethanesulfonimide lithium in methanol at room temperature for 30 h. The crude

product was concentrated and washed with water. The product was extracted from the aqueous phase using dichloromethane, then the phase was washed with distilled water until no residual chloride salt was detected with the use of $AgNO_3$. The phosphonium IL was dried in a vacuum at 80 °C for 6 h.

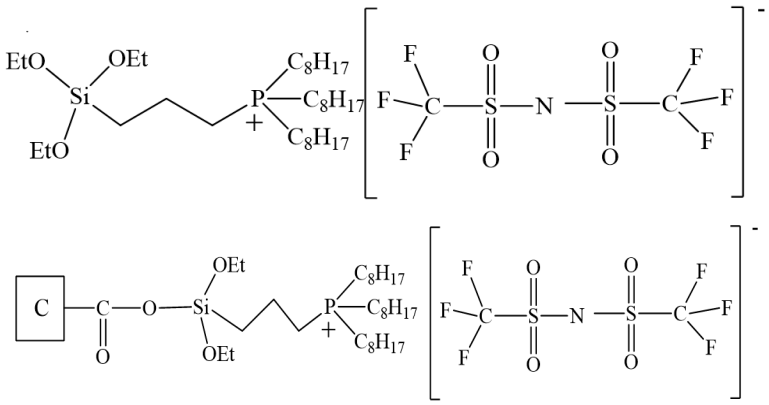

Figure 1. Molecular structure of phosphonium IL and IL-modified AC by grafting method.

The prepared phosphonium IL (1 or 2 g) was added to 10 mL anhydrous ethanol, respectively, then 1 g pretreated AC was added to the mixture. After standing at room temperature for 24 h, the samples were obtained by filtration and further dried at 80 °C under vacuum for 8 h. The product obtained was labeled as IPT-AC-1 or IPT-AC-2, respectively. The product obtained was confirmed by FTIR (Figure 2).

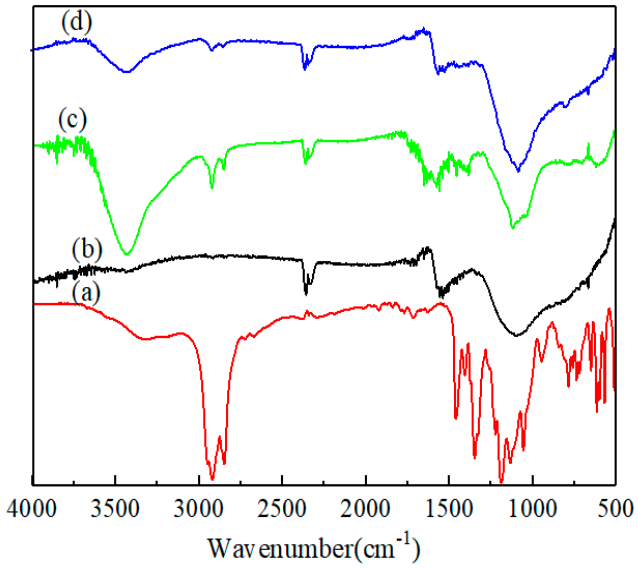

Figure 2. The FTIR spectra of phosphonium IL (a), AC (b), IPT-AC-1 (c) and GPT-AC-1 (d).

IR (γ max, cm^{-1}) of IPT-AC-1: 2922, 2850 cm^{-1} (C–H, aliphatic); 1384, 1339 cm^{-1} (S=O); 1355 cm^{-1} (P–C); 1227, 1194 cm^{-1} (C–F); 1134 cm^{-1} (Si–O); 667 cm^{-1} (S–C).

2.2.2. IL-Modified AC by Grafting Method

The pretreated AC was added into the mixture of 1 or 2 g prepared phosphonium ILs dissolved in 20 mL anhydrous ethanol. The mixture was stirred at a refluxing temperature for 36 h under the protection of nitrogen atmosphere. The solid was filtered and extracted with acetone under a reflux condition for 24 h via Soxhlet extraction. After vacuum drying at 95 °C for 8 h, the final adsorbent was obtained and coded as GPT-AC-1 or GPT-AC-2 (as shown in Figure 1), respectively. The product obtained was also confirmed by FTIR (Figure 2).

IR (γ max, cm^{-1}) of GPT-AC-1: 2920, 2850 cm^{-1} (C–H, aliphatic); 1349 cm^{-1} (P–C); 1134 cm^{-1} (Si–O); 1084 cm^{-1} (C–F); 668 cm^{-1} (S–C).

2.3. Characterizations

2.3.1. Chemical Analysis

Infrared spectrum analysis was carried out using a Thermo Scientific Nicolet 380 FTIR infrared spectrometer (Thermo Scientific, Waltham, MA, USA). An X-ray photoelectron spectroscopy measurement was performed on an X-ray photoelectron spectrometer ESCALAB 250Xi (Thermo Fisher Co, Waltham, MA, USA), and the binding energies were referenced to the neutral C1 speak at 284.8 eV. The surface was observed by S-3000N scanning electron microscope (Hitachi, Tokyo, Japan).

Using an STA409C DTA/DSC-TG (Netzsch, Selb, Germany), the thermal stability of the sample was analyzed at the heating rate of 10 °C/min in N_2 atmosphere. The IL loading amount on the surface of the AC was calculated by referring to the data measured with this instrument and assuming that all the weight lost in the 200–700 °C range belonged to the IL [25,26].

2.3.2. Evaluation of Pore Structure

The pore structures of the samples were confirmed by N_2 adsorption at −196 °C and CO_2 adsorption at 0 °C using an Autosorb-1-MP (Quantachrome, Boynton Beach, FL, USA). The sample was degassed at 150 °C and high vacuumed for 3 h to remove water and other volatile components. The pore size distribution (PSD) and pore structure parameters were obtained using density functional theory (DFT) with Quantachrome ASiQwin version 2.0 software (Quantachrome, NOVA2200e) based on the adsorption isotherms.

2.3.3. CO_2 Adsorption Performance

Adsorption selectivity of CO_2 and N_2 were measured on an IGA-003 Intelligent Gravimetric Analyzer (Hiden Isochema Ltd, Warrington, UK). The adsorption isotherms of CO_2 and N_2 were conducted at 25 °C and 0.1 MPa. Adsorption selectivity was the ratio of adsorption capacities in weight percentage for CO_2 versus N_2. More detailed information on the apparatus and analyzing methods have been reported in [27].

The dynamic adsorption and regeneration of mixed gases containing CO_2 15 vol.% and N_2 85 vol.% were carried out with a fixed bed column (7 mm inner diameter and 150 mm in height) apparatus (Figure 3). The CO_2 concentration at the outlet was analyzed by a GHX-3010E1 Infrared CO_2 Analyzer (Beijing Huayun Co, Beijing, China) with a given mixture of gas flow rate and pressure.

The dynamic adsorption was described through the concept of a breakthrough curve. The breakthrough and saturation point are defined as the point at which the outlet concentration from the column is about 5% or 95% of the inlet concentration respectively (c_0). Adsorption capacity (A) was defined as Equation (1).

The saturated adsorption capacity in the column is defined as Equation (1) [28]:

$$A = \frac{V}{mV_m} \tag{1}$$

where A denotes the CO_2-saturated adsorption amount of (mmol g^{-1}); m is the mass of the adsorbent (g); V is the volume of CO_2-saturated adsorption amount (m^3); and V_m is the standard molar volume at a standard temperature and pressure (0.1 MPa and 0 °C) (m^3/mol).

V can be calculated using the breakthrough curve according to Equation (2) [29]:

$$V = Q \int_{t_1}^{t_2} (c_2 - c_1) \mathrm{d}t \tag{2}$$

where Q is the gas flow rate (mL/min); c_1 and c_2 represent the outlet CO_2 concentrations at the breakthrough and saturation points during the adsorption process (vol.%), respectively; and t_1 and t_2 represent the time of the breakthrough point and saturation point (min), respectively.

The regeneration performance of IL-modified AC adsorbents was investigated by releasing pre-adsorbed CO_2 in inert N_2 at 100 °C for 1 h. The temperature of adsorbents was then cooled to 25 °C for the second adsorption.

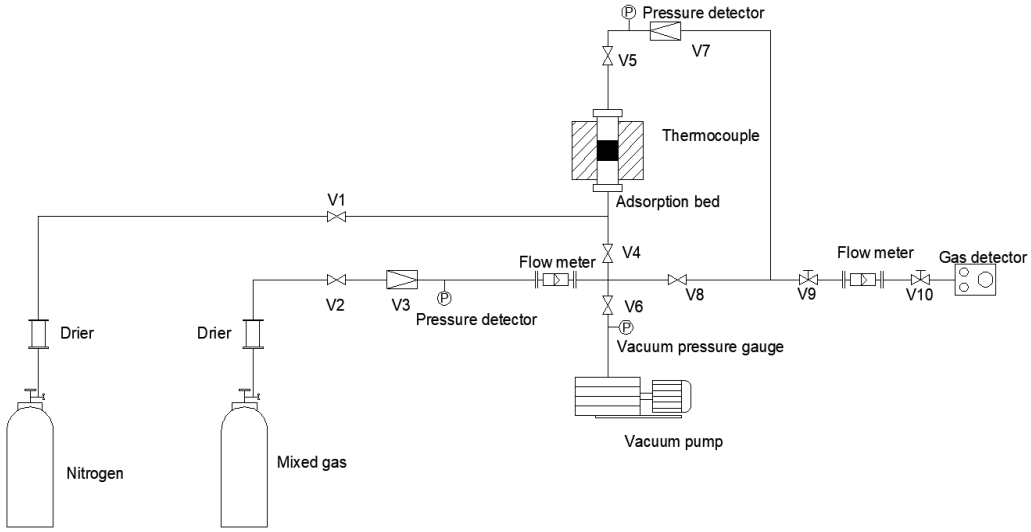

Figure 3. Schematic diagram of dynamic adsorption apparatus.

3. Results and Discussion

3.1. Characterization

3.1.1. X-ray Photoelectron Spectroscopy Analysis

Figure 4 displays the XPS spectrum of the surface of bare AC and GPT-AC-1. Only the peaks of C 1*s* and O 1*s* exist in the XPS spectrum of bare AC. The appearance of new peaks at 688.6, 397.7, 168.4, 132.9 and 103.5 eV are attributed to the F 1*s*, N 1*s*, S 2*p*, P 2*p* and Si 2*p* sourced from the IL, respectively. Therefore, the signal evidently shows that phosphonium IL has been grafted onto the silica surface.

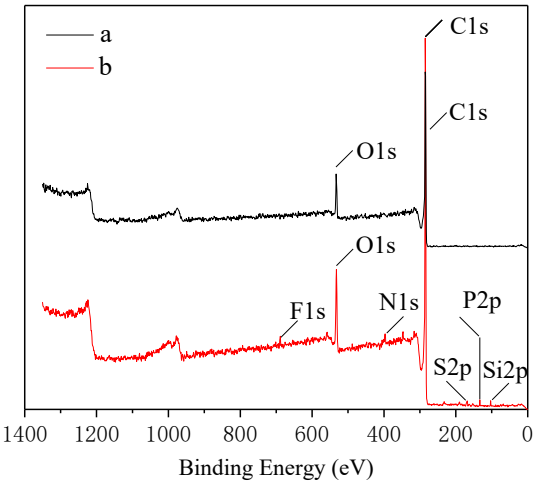

Figure 4. XPS spectrum of the surface of AC (a) and GPT-AC-1 (b).

3.1.2. Thermogravimetric Analysis

It has been proven that thermogravimetric analysis (TGA) is a useful technique for measuring the IL loading amount based on the weight loss of the adsorbent [30]. Figure 5 shows TGA curves of GPT-AC-1, GPT-AC-2, IPT-AC-1 and IPT-AC-2. The mass loss up to 200 °C corresponds to pre-adsorbed water and gas. According to the thermogravimetric curve observed in the range of 200–700 °C, the IL loading amount for GPT-AC-1, GPT-AC-2, IPT-AC-1 and IPT-AC-2 was 9.55, 9.85, 15.71 and 31.12 wt.%, respectively. The impregnation method can significantly increase the IL loading amount, while the grafting method restricts the IL loading due to the limited number of groups on the AC surface.

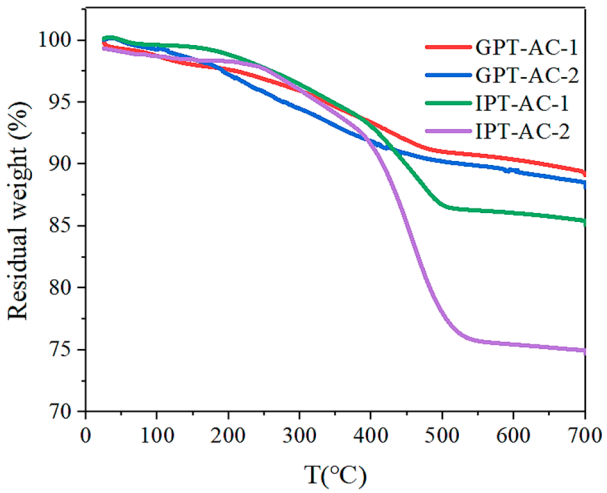

Figure 5. Thermogravimetric (TGA) curves of GPT-AC-1, GPT-AC-2, IPT-AC-1 and IPT-AC-2.

3.1.3. Scanning Electron Microscope (SEM) Analysis

Figure 6 displays a scanning electron morphology of activated carbon-supported IL. The pore structure of GPT-AC-2 prepared by the grafting method was well developed due to chemical bond on the surface of the carrier, which had little effect on the pore structure. Meanwhile, IPT-AC-1 prepared via the impregnation method was relatively less porous, and the ordered pores could hardly be observed. A higher IL loading may have blocked the pores, leading to a more serious plugging phenomenon. It is also obvious that the pores of IPT-AC-1 were packed with a thin IL film.

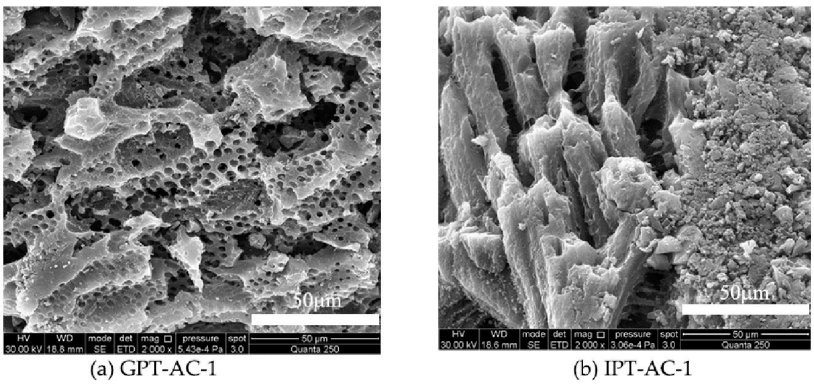

(a) GPT-AC-1 (b) IPT-AC-1

Figure 6. SEM images of GPT-AC-1(**a**) andIPT-AC-1 (**b**).

3.1.4. Evaluation of Pore Structure

The pore structure parameters and pore size distribution were obtained based on the N_2 sorption isotherm, as illustrated in Table 1. As shown in Table 1, the pores of AC modified by IL were mainly micropores, which are favorable for CO_2 adsorption. The micropores in AC have made a great

contribution to the adsorption of CO_2 [31]. The grafted samples GPT-AC-1 and GPT-AC-2 were superior to the impregnated samples in pore volume and specific surface area, which was a result of the lower IL loading amounts by the grafted samples in combination with TGA. As the IL loadings increased, the pores reduced more, and it is this proven that the grafting method can better maintain the specific surface area and accumulated pore structure of the carrier, which was also confirmed by the SEM analysis.

Table 1. Pore structure parameters of IL-modified AC using N_2 sorption.

Sample	Distribution of Pore Volume with Aperture-Width		CPV	CSA
	0–2 (nm)	2–24 (nm)	($cm^3 \cdot g^{-1}$)	($m^2 \cdot g^{-1}$)
GPT-AC-1	72.775%	27.225%	0.318	502.0
GPT-AC-2	70.574%	29.426%	0.334	549.6
IPT-AC-1	65.825%	34.175%	0.263	431.3
IPT-AC-2	48.078%	51.922%	0.191	277.6

CPV—cumulative pore volume; CSA—cumulative specific surface area.

CO_2 was used as the adsorbed substance to fill the micropores in the adsorbent, which is more suitable for analysis of microporous structures [32,33]. The micropore size distribution of each sample was obtained according to the adsorption isotherms of CO_2, as shown in Figure 7. The *y*-axis in Figure 7 indicates the rate of change of the pore volume v (cm^3/g) according to the pore dimensionality d_p (nm). The pore size of all samples was mostly in the range of 0.2–1.0 nm.

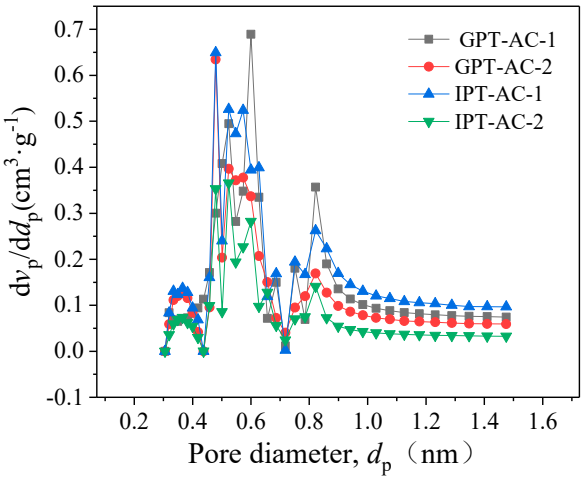

Figure 7. Micropore size distribution of all samples using CO_2 sorption.

3.2. CO_2/N_2 Selectivity

Figure 8 shows the CO_2 and N_2 adsorption capacity and CO_2/N_2 selectivity at 0.1 MPa and 25 °C. It is observed that all IL-modified AC had better adsorption selectivity of CO_2/N_2 in comparison with bare AC. With the increase of IL loading, the selectivity of the samples increased gradually as well. In particular, IPT-AC-1 and IPT-AC-2 prepared by the impregnation method had better CO_2/N_2 selectivity due to a higher IL loading amount on the surface of the AC.

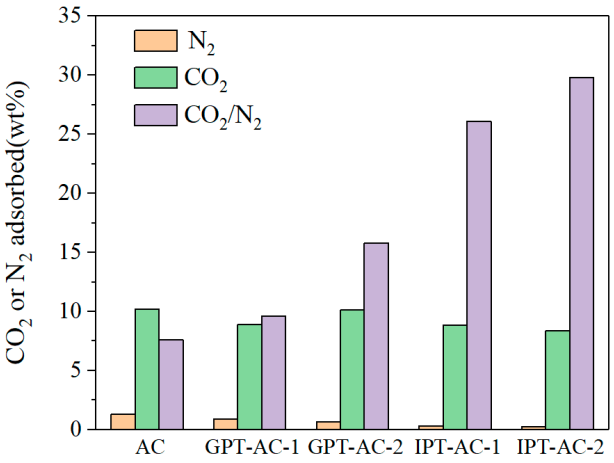

Figure 8. Adsorbed CO_2 and N_2, and CO_2/N_2 selectivity of IL-modified AC at 25 °C and 0.1 MPa.

Since IL covering the surface of the carrier can form a layer of thin film, it can permit CO_2 adsorption and effectively block the entry of N_2 (as shown in Figure 9). It is worth noting that for IPT-AC-1 and IPT-AC-2, IL loading of the latter was twice as much as that of the former, but the selectivity was not significantly improved. This may have been due to excessive IL loading that blocked the channel, as determined through pore structure analysis. The blockage of pores leads to a decrease of the specific surface area and cumulative pore volume (CPV), which in turn leads to a decrease in CO_2 adsorption capacity.

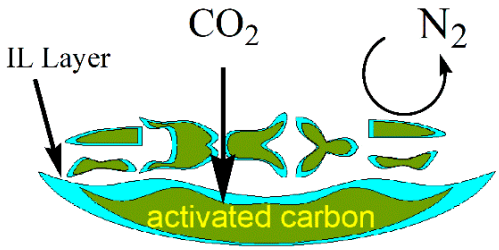

Figure 9. The schematic diagram of phosphonium IL modified AC blocking N_2.

Therefore, the selection of the appropriate immobilization method and IL loading can improve the surface performance and pore structure of AC. By maintaining a large specific surface area and cumulative pore volume and a suitable IL layer, a higher CO_2 adsorption performance can be obtained.

3.3. Dynamic Adsorption Performance

Gas flow rate and adsorption pressure are important operational parameters in determining the efficiency of adsorbents in the continuous process of industrial treatment. The dynamic adsorption properties of GPT-AC-2 and IPT-AC-1 in the gas mixture containing 15 vol.% CO_2 and balanced N_2 were investigated. The influences of flow rates and pressure on the CO_2 breakthrough curves are shown in Figures 10 and 11.

3.3.1. Effect of Flow Rate

As shown in Figure 10, the breakthrough points of GPT-AC-2 and IPT-AC-1 decreased at high flow rates where the breakthrough curves shifted toward the origin. When the flow rate increased to a high value, the space time of the gaseous adsorbent was shortened, leading to earlier adsorbate penetration.

Higher flow rates might have also strengthened mass transfer and made the breakthrough curve of both samples steeper. It is worth noting that the breakthrough curve of IPT-AC-1 was relatively flat. The steepness of the breakthrough curve indicates the magnitude of mass transfer resistance, and a

steeper curve indicates a smaller mass transfer resistance. In Figure 10, it can be seen that the mass transfer resistance of GPT-AC-2 is low.

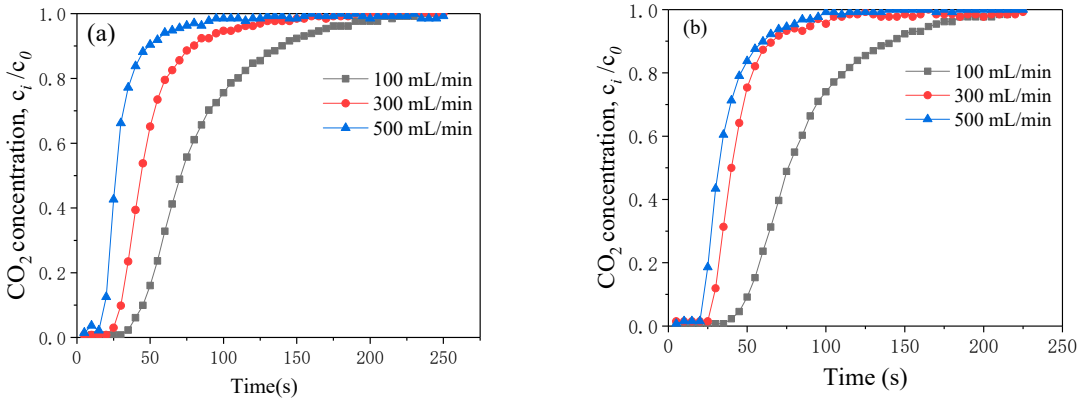

Figure 10. CO_2 breakthrough curves of GPT-AC-2 (**a**) and IPT-AC-1 (**b**) at 0.2 MPa and 25 °C.

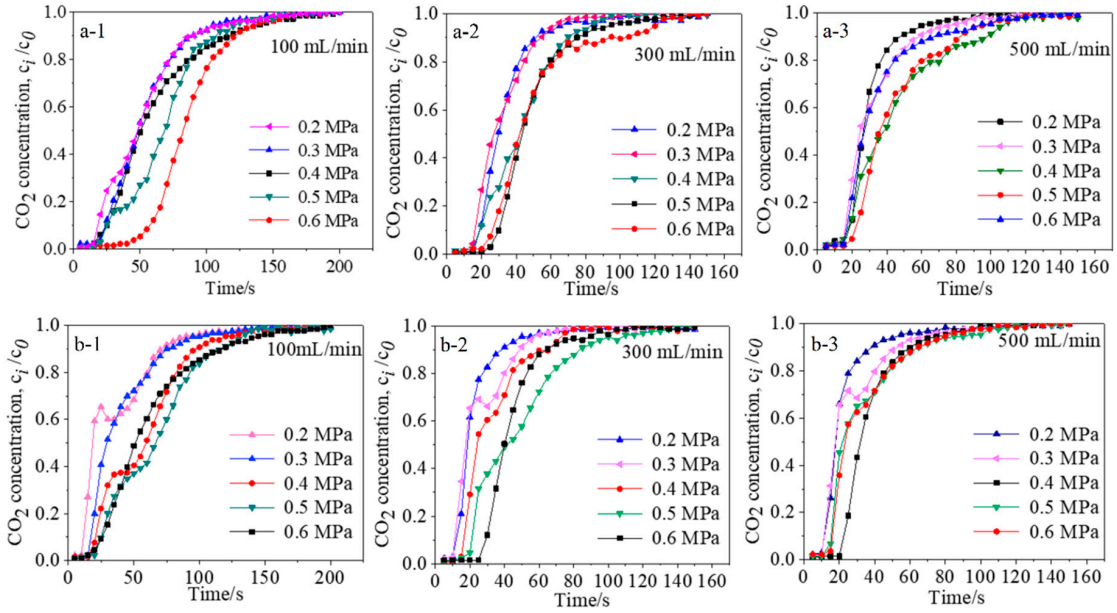

Figure 11. Breakthrough curves of GPT-AC-2 at 100 mL/min (**a–1**), 300 mL/min (**a–2**), 500 mL/min (**a–3**); IPT-AC-1 at 100 mL/min (**b–1**), 300 mL/min (**b–2**), 500 mL/min (**b–3**).

For porous adsorbents, CO_2 adsorption diffusion may be very important. In the range of experimental gas flow rates, the diffusion process of CO_2 on adsorbents consists of gas film diffusion and intra-particle diffusion [34–36]. The mass transfer resistance of gas film is affected by flow rate and pressure, and the intra-particle diffusion resistance is determined by the pore structure of adsorbents [37]. When the flow rate is kept at lower value, the gas film diffusion may be an important rate-controlling step in the CO_2 adsorption process. The longer the gas stays in the adsorption bed, the more sufficient the gas is on the adsorbents, which is beneficial to the diffusion into the pore channel. Under the same experimental conditions, the external diffusion resistance of two modified samples is not significantly different, but the intra-particle diffusion resistance is significantly different due to the difference of micropore structure. Combined with the porosity analysis and SEM analysis of the two samples, the pore structure of GPT-AC-2 is more developed and the blockage of IL in the pore is lessened, leading to low mass transfer resistance of GPT-AC-2 in the pore.

3.3.2. Effect of Adsorption Pressure

To express the effect of pressure, the breakthrough curves of two adsorbents in CO_2/N_2 mixture in the range of pressure from 0.2 to 0.6 MPa at a given gas flow rate are compared (as shown in Figure 11). It is worth noting that the effect of pressure on the breakthrough curves for GPT-AC-2 and IPT-AC-1 are different.

The overall tendency for GPT-AC-2 is that a higher pressure leads to the breakthrough curves shifting towards the right and a longer breakthrough time, especially at lower gas flow rates, because of a decrease in the mean free s, the breakthrough time does not always increase. Moreover, the breakthrougpath of gas at higher pressures. However, as the pressure continuously increases at higher flow rateh curves become obviously steeper with an increase in pressure, especially at lower flow rates.

The breakthrough curves of IPT-AC-1 show that the effect of pressure is similar to that of GPT-AC-2, but there are obvious differences in behavior at 100 and 300 mL/min. There is no significant change in the breakthrough point with an increase of pressure at a flow rate of 100 mL/min, while longer penetration and breakthrough time occur at 300 mL/min. It is also observed that with an increase of pressure, the steepness of the breakthrough curve is also varied at different flow rates, indicating that IPT-AC-1 with a higher IL loading may possess a more complicated mass transfer resistance than GPT-AC-2.

3.3.3. Adsorption Capacity

CO_2-saturated adsorption amounts of GPT-AC-2 and IPT-AC-1 based on breakthrough curves are presented in Table 2. A reduction of breakthrough time by increasing the flow rate reflects a reduction in adsorption; for example, the CO_2 adsorption capacity for GPT-AC-2 decreased from 1.105 to 0.748 mmol·g^{-1} at 0.2 MPa when the flow rate increased from 100 to 500 mL/min, while decreasing from 0.872 to 0.681 mmol·g^{-1} for IPT-AC-1.

Table 2. CO_2-saturated adsorption capacities of GPT-AC-2 and IPT-AC-1.

Pressure (MPa)	GPT-AC-2 Adsorption (mmol·g^{-1})	IPT-AC-1 Adsorption (mmol·g^{-1})	GPT-AC-2 Adsorption (mmol·g^{-1})	IPT-AC-1 Adsorption (mmol·g^{-1})	GPT-AC-2 Adsorption (mmol·g^{-1})	IPT-AC-1 Adsorption (mmol·g^{-1})
	100 mL/min		300 mL/min		500 mL/min	
0.2	1.105	0.872	0.843	0.731	0.748	0.681
0.3	1.134	0.893	0.877	0.752	0.824	0.723
0.4	1.278	1.181	1.157	0.815	1.112	0.925
0.5	1.383	1.323	1.268	1.106	1.221	0.839
0.6	1.746	1.240	1.335	1.133	0.856	0.832

The CO_2 adsorption capacity increased with increasing pressure, while there was no obvious effect at higher pressures or gas flow rates. The adsorption capacity of GPT-AC-2 enhanced from 1.105 to 1.746 mmol·g^{-1} at a 100 mL/min flow rate with increasing pressure from 0.2 to 0.6 MPa. It is noticed that the effect of pressure on CO_2 adsorption capacity for IPT-AC-1 was slightly different at higher pressures. This clearly indicates that there is a corresponding optimal operating condition for phosphonium IL-modified AC prepared with different methods.

4. Conclusions

Phosphonium-based IL was immobilized on AC by grafting and impregnation methods, and CO_2 and N_2 sorption behavior of modified samples as investigated and compared with a bare AC. It was suggested that the ionic liquid was successfully and firmly immobilized on AC, and the IL-impregnated sample provided a higher IL-selecting film for CO_2/N_2 separation. The adsorption capacity and breakthrough curves of CO_2 on modified AC were further investigated at different pressures and gas flow rates by the dynamic column breakthrough method. The functionality by covalent grafting

provided a higher micropore, showing higher CO_2 dynamic adsorption and mass transfer. This could allow for the adjustment of the IL phase and alter the operating conditions of adsorption processes by achieving a better CO_2-selective adsorption.

Author Contributions: Conceptualization, X.H. and J.Z.; methodology, X.H.; writing—original draft preparation, X.H. and H.W.; writing—review and editing, J.Z.; data curation, M.Z. and S.Z.

Funding: The authors would like to thank the financial support of the Fundamental Research Funds for the Central Universities, NO. 2019XKQYMS14.

Acknowledgments: The authors wish to acknowledge Lifang Zhang for providing the thermal analysis and pore structure analysis for the adsorbents used in the present study.

Conflicts of Interest: The authors declare no conflict of interest.

References

1. Chaffee, A.L.; Knowles, G.P.; Liang, Z.; Zhang, J.; Xiao, P.; Webley, P.A. CO_2 capture by adsorption: Materials and process development. *Int. J. Greenh. Gas Control* **2007**, *1*, 11–18. [CrossRef]
2. Abbaspour Tamijani, A.; Ebrahimiaqda, E. Facet of rutile-structured GeO_2: An ab initio investigation. *Mol. Phys.* **2017**, *115*, 1598–1605. [CrossRef]
3. Corum, W.K.; Abbaspour Tamijani, A.; Mason, E.S. Density functional theory study of arsenate adsorption onto alumina surfaces. *Minerals* **2018**, *8*, 91. [CrossRef]
4. Jones, C.W. CO_2 capture from dilute gases as a component of modern global carbon management. *Annu. Rev. Chem. Biomol. Eng.* **2011**, *2*, 31–52. [CrossRef] [PubMed]
5. El Gamal, M.; Mousa, H.A.; El-Naas, M.H.; Zacharia, R.; Judd, S. Bio-regeneration of activated carbon: A comprehensive review. *Sep. Purif. Technol.* **2018**, *197*, 345–359. [CrossRef]
6. Pevida, C.; Plaza, M.G.; Arias, B.; Fermoso, J.; Rubiera, F.; Pis, J.J. Surface modification of activated carbons for CO_2 capture. *Appl. Surf. Sci.* **2008**, *254*, 7165–7172. [CrossRef]
7. Shafeeyan, M.S.; Daud, W.M.A.W.; Houshmand, A.; Shamiri, A. A review on surface modification of activated carbon for carbon dioxide adsorption. *J. Anal. Appl. Pyrolysis* **2010**, *89*, 143–151. [CrossRef]
8. Rehman, A.; Park, M.; Park, S.J. Current progress on the surface chemical modification of carbonaceous materials. *Coatings* **2019**, *9*, 103. [CrossRef]
9. Durán, I.; Álvarez-Gutiérrez, N.; Rubiera, F.; Pevida, C. Biogas purification by means of adsorption on pine sawdust-based activated carbon: Impact of water vapor. *Chem. Eng. J.* **2018**, *353*, 197–207. [CrossRef]
10. Zhang, Y.; Ji, X.; Xie, Y.; Lu, X. Screening of conventional ionic liquids for carbon dioxide capture and separation. *Appl. Energy* **2016**, *162*, 1160–1170. [CrossRef]
11. Aghaie, M.; Rezaei, N.; Zendehboudi, S. A systematic review on CO_2 capture with ionic liquids: Current status and future prospects. *Renew. Sustain. Energy Rev.* **2018**, *96*, 502–525. [CrossRef]
12. Zhang, X.; Zhang, X.; Dong, H.; Zhao, Z.; Zhang, S.; Huang, Y. Carbon capture with ionic liquids: Overview and progress. *Energy Environ. Sci.* **2012**, *5*, 6668–6681. [CrossRef]
13. Hemp, S.T.; Zhang, M.; Allen, M.H., Jr.; Cheng, S.; Moore, R.B.; Long, T.E. Comparing ammonium and phosphonium polymerized ionic liquids: Thermal analysis, conductivity, and morphology. *Macromol. Chem. Phys.* **2013**, *214*, 2099–2107. [CrossRef]
14. Ficke, L.E.; Novak, R.R.; Brennecke, J.F. Thermodynamic and thermophysical properties of ionic liquid + water systems. *J. Chem. Eng. Data* **2010**, *55*, 4946–4950. [CrossRef]
15. Neves, C.M.S.S.; Carvalho, P.J.; Freire, M.G.; Coutinho, J.A.P. Thermophysical properties of pure and water-saturated tetradecyltrihexylphosphonium-based ionic liquids. *J. Chem. Thermodyn.* **2011**, *43*, 948–957. [CrossRef]
16. Xie, W.; Ji, X.; Feng, X.; Lu, X. Mass-transfer rate enhancement for CO_2 separation by ionic liquids: Theoretical study on the mechanism. *AIChE J.* **2015**, *61*, 4437–4444. [CrossRef]
17. Ren, J.; Li, Z.; Chen, Y.; Yang, Z.; Lu, X. Supported ionic liquid sorbents for CO_2 capture from simulated flue-gas. *Chin. J. Chem. Eng.* **2018**, *26*, 2377–2384. [CrossRef]
18. Zulkurnai, N.Z.; Ali, U.M.; Ibrahim, N.; Abdul Manan, N.S. Carbon Dioxide (CO_2) adsorption by activated carbon functionalized with deep eutectic solvent (DES). *IOP Conf. Ser. Mater. Sci. Eng.* **2017**, *206*, 012001. [CrossRef]

19. D'Alessandro, D.M.; Smit, B.; Long, J.R. Carbon dioxide capture: Prospects for new materials. *Angew. Chem. Int. Ed.* **2010**, *49*, 6058–6082. [CrossRef]
20. Lin, K.Y.A.; Park, A.H.A. Effects of bonding types and functional groups on CO_2 capture using novel multiphase systems of liquid-like nanoparticle organic hybrid materials. *Environ. Sci. Technol.* **2011**, *45*, 6633–6639. [CrossRef] [PubMed]
21. Kinik, F.P.; Altintas, C.; Balci, V.; Koyuturk, B.; Uzun, A.; Keskin, S. [BMIM][PF6] incorporation doubles CO_2 selectivity of ZIF-8: Elucidation of interactions and their consequences on performance. *ACS Appl. Mater. Interfaces* **2016**, *8*, 30992–31005. [CrossRef]
22. Ruckart, K.N.; O'Brien, R.A.; Woodard, S.M.; West, K.N.; Glover, T.G. Porous solids impregnated with task-specific ionic liquids as composite sorbents. *J. Phys. Chem. C* **2015**, *119*, 20681–20697. [CrossRef]
23. Erto, A.; Silvestre-Albero, A.; Silvestre-Albero, J.; Rodríguez-Reinoso, F.; Balsamo, M.; Lancia, A.; Montagnaro, F. Carbon-supported ionic liquids as innovative adsorbents for CO_2 separation from synthetic flue-gas. *J. Colloid Interface Sci.* **2015**, *448*, 41–50. [CrossRef]
24. Zhu, J.; Xin, F.; Huang, J.; Dong, X.; Liu, H. Adsorption and diffusivity of CO_2 in phosphonium ionic liquid modified silica. *Chem. Eng. J.* **2014**, *246*, 79–87. [CrossRef]
25. El-Hendawy, A.N.A. Influence of HNO_3 oxidation on the structure and adsorptive properties of corncob-based activated carbon. *Carbon* **2003**, *41*, 713–722. [CrossRef]
26. Green, M.D.; Salas-de la Cruz, D.; Ye, Y.; Layman, J.M.; Elabd, Y.A.; Winey, K.I.; Long, T.E. Alkyl-substituted N-vinylimidazolium polymerized ionic liquids: Thermal properties and ionic conductivities. *Macromol. Chem. Phys.* **2011**, *212*, 2522–2528. [CrossRef]
27. Liu, H.; Huang, J.; Pendleton, P. Experimental and modelling study of CO_2 absorption in ionic liquids containing Zn (II) ions. *Energy Procedia* **2011**, *4*, 59–66. [CrossRef]
28. Li, G.; Wang, Q.; Jiang, T.; Luo, J.; Rao, M.; Peng, Z. Roll-up effect of sulfur dioxide adsorption on zeolites FAU 13X and LTA 5A. *Adsorption* **2017**, *23*, 699–710. [CrossRef]
29. Kaur, B.; Gupta, R.K.; Bhunia, H. Chemically activated nanoporous carbon adsorbents from waste plastic for CO_2 capture: Breakthrough adsorption study. *Microporous Mesoporous Mater.* **2019**, *282*, 146–158. [CrossRef]
30. Bernard, F.L.; Duczinski, R.B.; Rojas, M.F.; Fialho, M.C.C.; Carreño, L.Á.; Chaban, V.V.; Vecchia, F.D.; Einloft, S. Cellulose based poly(ionic liquids): Tuning cation-anion interaction to improve carbon dioxide sorption. *Fuel* **2018**, *211*, 76–86. [CrossRef]
31. Huang, G.G.; Liu, Y.F.; Wu, X.X.; Cai, J.J. Activated carbons prepared by the KOH activation of a hydrochar from garlic peel and their CO_2 adsorption performance. *New Carbon Mater.* **2019**, *34*, 247–257. [CrossRef]
32. Wu, F.C.; Wu, P.H.; Tseng, R.L.; Juang, R.S. Description of gas adsorption isotherms on activated carbons with heterogeneous micropores using the Dubinin–Astakhov equation. *J. Taiwan Inst. Chem. Eng.* **2014**, *45*, 1757–1763. [CrossRef]
33. Gibson, J.A.A.; Gromov, A.V.; Brandani, S.; Campbell, E.E.B. The effect of pore structure on the CO_2 adsorption efficiency of polyamine impregnated porous carbons. *Microporous Mesoporous Mater.* **2015**, *208*, 129–139. [CrossRef]
34. Lively, R.P.; Leta, D.P.; DeRites, B.A.; Chance, R.R.; Koros, W.J. Hollow fiber adsorbents for CO_2 capture: Kinetic sorption performance. *Chem. Eng. J.* **2011**, *171*, 801–810. [CrossRef]
35. Guo, Y.; Zhao, C.; Li, C.; Wu, Y. CO_2 sorption and reaction kinetic performance of K_2CO_3/AC in low temperature and CO_2 concentration. *Chem. Eng. J.* **2015**, *260*, 596–604. [CrossRef]
36. Álvarez-Gutiérrez, N.; Gil, M.V.; Rubiera, F.; Pevida, C. Kinetics of CO_2 adsorption on cherry stone-based carbons in CO_2/CH_4 separations. *Chem. Eng. J.* **2017**, *307*, 249–257. [CrossRef]
37. Guo, Y.; Tan, C.; Wang, P.; Sun, J.; Yan, J.; Li, W.; Zhao, C.; Lu, P. Kinetic study on CO_2 adsorption behaviors of amine-modified co-firing fly ash. *J. Taiwan Inst. Chem. Eng.* **2019**, *96*, 374–381. [CrossRef]